Advances in Geo-Energy Research

Vol. 12, No. 3, p. 194-204, 2024

Invited review

Expanding role of borehole image logs in reservoir fracture and heterogeneity characterization: A review

David A. Wood*

DWA Energy Limited, Lincoln LN5 9JP, UK

Keywords:
Borehole imaging tools
fracture characteristics
automated fracture detection
horizontal stresses
reservoir anisotropy
integrated borehole imaging analysis

Cited as:
Wood, D. A. Expanding role of borehole image logs in reservoir fracture and heterogeneity characterization: A review. Advances in Geo-Energy Research, 2024, 12(3): 194-204.
https://doi.org/10.46690/ager.2024.06.04

Abstract:
Borehole imaging well-log datasets provide a wide range of valuable information for various aspects of petroleum reservoir characterization. In particular, electrical borehole images make it possible to detect and quantify the distributions, orientations, and forms of fractures at high resolution. Acoustic borehole images are extensively used for breakout detection and width measurements to determine horizontal principal stress magnitudes and orientations. However, by combining information from different types of borehole imaging tools more comprehensive reservoir characterization can be achieved. Data from the dipole shear-wave imager can be used to provide anisotropy insights that are of complementary value for lithofacies, poro-permeability, and seismic dataset interpretations of heterogeneous reservoirs. Cases are made to incorporate data from both electrical and acoustic borehole imaging datasets into integrated reservoir characterization analysis. Moreover expanding the reach of borehole imaging data is becoming increasingly possible with the aid of machine learning models configured to predict key borehole imaging metrics from standard suites of petrophysical well-log and drilling mud-log datasets.

1. Introduction

Fractures occur in reservoir formations as natural and artificially induced phenomena and are of particular interest because of their contribution to porosity/permeability in otherwise tight heterogeneous formations of limestone (Boro et al., 2014; Hosseinzadeh et al., 2023), sandstone (Faraji et al., 2020), shale (Ismail et al., 2024) and coal seams (Wood and Cai, 2022). However, fluid-flow predictions from fractured formations are difficult to generate from multi-phase-flow models incorporating geomechanical information derived from rock cores (Hawez et al., 2021). The reason for this is the sporadic and uneven distribution of fracture zones and fluctuations in principal stress magnitudes and directions across complex structural and stratigraphic traps (Fanchi, 2018). However, if fracture clusters can be identified with confidence they frequently correlate with the most productive zones in many reservoirs. Hence, reliable fracture characterization and distribution prediction can be a valuable field exploration and development tool.

Discrete fracture network models require accurate fracture characterization details to provide meaningful reservoir simulation results. Fracture/fault detection, orientation, and characterization can be predicted with the aid of borehole imaging (BHI) well-log tools verified with core data (Hosseinzadeh et al., 2023) and then predicted using various machine learning methods (Tabasi et al., 2022; Vijouyeh et al., 2023). Information from BHI tools has been widely used since their development more than four decades ago (Bourke et al., 1989), particularly for quantitative fracture-characterization purposes (Luthi and SSouhaité, 1990). In recent years, it has been demonstrated that faulting, fracture orientation (Zhou et al., 2022), fracture density (Tóth et al., 2023), geomechanical rock properties (Vahle et al., 2020), reservoir stress magnitudes and orientations (Faraji et al., 2020), and fracture dimensions (Vijouyeh et al., 2023) can all be effectively quantified by the use of borehole-image information. BHI data usefully complements sparsely available core data because it can be recorded

Yandy Scientific Press

*Corresponding author.
E-mail address: dw@dwasolutions.com (D. A. Wood).

Received April 12, 2024; revised May 2, 2024; accepted May 24, 2024; available online May 28, 2024.

continuously over extensive depth intervals and, depending on the BHI tool used, can record wellbore features at high resolutions. By exploiting supervised machine learning models trained with BHI data, verified with some core information, to predict various fracture characteristics, it is possible to integrate such models within reservoir simulations to function as proxy or surrogate models, saving time and cost (Ng et al., 2023).

Convolutional neural networks (CNN) are now applied to directly detect fractures and linear features from BHI data (Krizhevsky et al., 2017), when supervised with a training set of annotated images. Subsequent developments involving fast-region CNN (Dias et al., 2020) and Mask-R CNN (Liu et al., 2022) and improved image pre-processing sequences (Du et al., 2023) have further improved the functionality of automated feature detection from BHI datasets.

However, BHI data can provide a much broader spectrum of useful information for reservoir characterization than fracture analysis. By combining information from different types of BHI tools, together with core, petrophysical, and mud-logging data it is possible to characterize heterogeneous and anisotropic reservoirs more comprehensively. In particular, the use of shear-wave data extracted from the dipole shear wave sonic imager can provide valuable information regarding the magnitude and orientation of anisotropy in complex reservoir formations (Sadeqi et al., 2022). The objective of this study is to describe the broad range of capabilities of BHI data concerning reservoir characterization and illustrate the benefits of using that data as part of an integrated reservoir analysis. Published sources that provide the equations and further details of methods used in the quantitative analysis of BHI data are listed in the Supplementary file.

2. Types of borehole imaging devices

Although there are many different BHI tools offered by drilling service companies, those tools fall within two main categories: electrical BHI tools and acoustic (ultrasound) BHI tools. These two types of BHI detect different types of features to different resolutions. The manufacturers' specifications highlight the higher resolutions of the electrical BHI tool can detect features at scales of approximately 50 μm (SLB, 2024), whereas the acoustic tools can distinguish features of approximately 1 cm thickness (IODP, 2024).

The formation micro-imager (FMI) is a wire-line electrical BHI tool (SLB, 2024; note that SLB is the name of the former service company "Schlumberger"). The FMI directs electrical currents at the walls of the borehole and detects/records the electric currents induced processing/converting those signals into spatially oriented assembled images (Ekstrom et al., 1986). The tool is effective in a wide range of borehole conditions and drilling fluid types (Brown et al., 2015). It extends and places four equidistant arms from the lower part of the tool with pads and flaps and places them close to the wellbore wall. Each arm carries 48 source electrodes (192 in total) (Nabiei et al., 2021). In ideal borehole conditions, and according to the tool manufacturers' claims, the tool achieves about eighty percent coverage of the wellbore wall and assembles eight continuous strips of images along the wellbore each with a specified orientation. The other major service companies offer comparable tools. For example, Halliburton (2024) offers its X-tended Range Micro Imaging (XRMI™) tool, and Weatherford (2024) offers its Compact™ Microresistivity Tool.

The formation micro-scanner (FMS) is a lower specification alternative to the FMI with each of its four pads carrying 16 source electrodes (64 in total). The FMS samples current intensity every 2.5 mm and covers about fifty percent of the wellbore circumference (Columbia University, 2024). The features detected by the FMI and FMS tools can be accurately calibrated with data from rock cores where it is available (Khoshbakht et al., 2012). However, the high-resolution coverage provided by these tools goes far beyond what can be covered by fragmentary rock cores, as these BHI tools can be run to survey thousands of meters of wellbore wall. The FMI and FMS resolutions are adequate to detect fractures and micro-fractures with precision.

There are several acoustic BHI tools offered by different service companies but all essentially provide similar ultrasound images that cover 360 degrees of the borehole wall because the acoustic transducers rotate a high speeds as the tools record their signals. The ultrasonic borehole imager (UBI), offered by SLB, operates at high frequencies: 250 KHz to deliver an image resolution of 1.02 cm; or 500 kHz to deliver an image resolution of 0.51 cm (IODP, 2024).

The acoustic images provided by these tools are of sufficient resolution to delineate wellbore breakouts and survey wellbore-stability detection purposes. In addition, detailed reservoir analysis of ultrasonic image logs is also possible. For example, it is possible to invert the 360° porosity spectrum for large depth intervals from ultrasonic BHI tools combined with standard wireline log petrophysical data (Zhang et al., 2018), demonstrating good agreement with direct porosity measurements. This technique is particularly useful in heterogeneous carbonate reservoirs.

The circumferential borehole imaging tool (CBIT), offered by Baker Hughes, is designed to operate and generate interpretable acoustic images in a wide range of borehole conditions including those with casing in place and with large and irregular diameters (LandSea, 2024). It operates at 250 kHz and records and processes magnitude (amplitude) signals and travel-time signals displaying each as images.

The dipole shear sonic imager (DSI) tool is a full-waveform acoustic imaging tool, offered by Schlumberger (now traded under the company name SLB) (Columbia University, 2024). The DSI tool generates a range of frequencies from two orthogonal-dipole transmitters and a single monopole transmitter (Esmersoy et al., 1995). It records signals from the wellbore wall and beyond with an eight-receiver array. The DSI and FMS tools are sometimes run in combination to provide both electrical and acoustic images. The DSI generates part of its acoustic signal at high frequency (8 to 30 kHz bandwidth). These signals induce both compressional and shear waves through the formation adjacent to the wellbore recordings as they are transmitted through rock formations. The two dipole transmitters emit lower-frequency pulses (80 Hz to 1.5 kHz

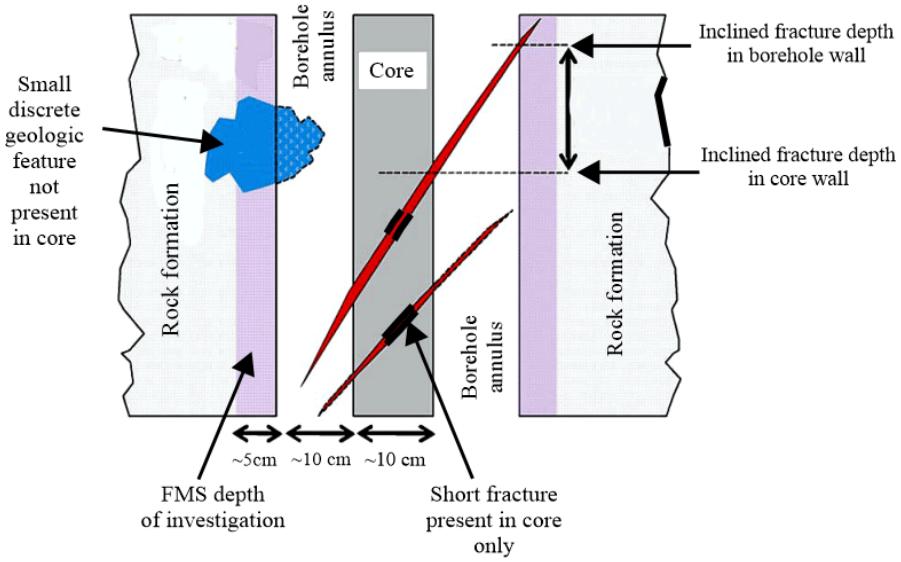

Fig. 1. Diagram representing features that may appear differently in wellbore cores and borehole wall images recovered from the same depth intervals. Modified from Khoshbakht et al. (2012).

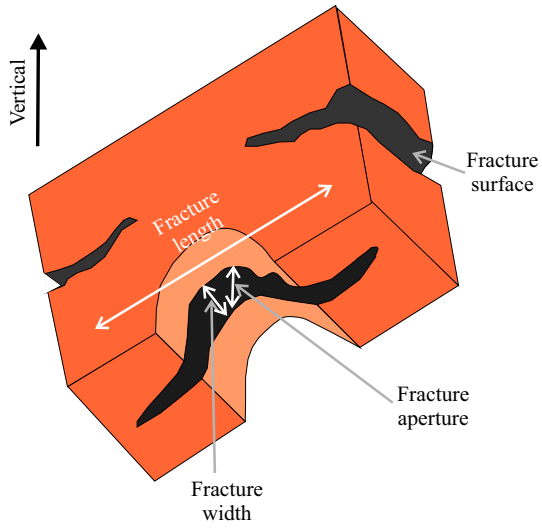

Fig. 2. Terminology and form of rock-formation fractures.

bandwidth) that create mainly shear waves within the adjacent formations, plus low-frequency pulses (~5 kHz) which function specifically to generate more deeply penetrating Stoneley waves (Qobi et al., 2001; Haldorsen et al., 2006). DSI-generated acoustic recordings can be processed and interpreted to provide stress anisotropy conditions in adjacent rock formations (Pachineelam et al., 2011).

Other trademarked BHI tools work on similar principles to the four tools briefly described (FMI, DSI, UBI, and CBIT) and deliver similar types of images. In addition, some Chinese companies now offer BHI tools (e.g. Chongqing Gold Mechanical & Electrical Equipment, 2024), although these are yet to rival the tools offered by the international service companies for worldwide borehole applications. The capabilities of the different types of BHI tools are described and illustrated in the following sections with the aid of published image examples of selected tools applied in specific wellbores.

3. Features observed in cores versus borehole images

Wellbore features that are imaged by BHI logs are not identical to those observed in cores from the same depth section of a wellbore, for the reasons illustrated in Fig. 1.

Typically there is a difference in diameters between recovered cores and the full wellbore of between about 10 and 20 cm. This width disparity results in certain features being detected at different depths in cores and by BHI tools or only being detected in one and not the other. Moreover, cores only rarely involve 100% recovery and there are some gaps in the wellbore wall surveys conducted by electrical BHI tools (50% to 80% based on tool manufacturers' claims depending upon the specific recording tool used and borehole conditions).

4. Fracture characteristics discernible in borehole images

Fractures in rock formations have unique characteristics that provide valuable information about the formations and their stress conditions. Figs. 2 and 3 describe some of the fundamental characteristics of fractures that are discernible and measurable in cores and BHI datasets.

Although fractures are planar features they rarely have uniquely linear trajectories along their entire lengths displaying asperities and with surfaces that are not smooth when studied in detail. They may also be filled or partly filled by diagenetic minerals (Fanchi, 2018), or empty and open. These factors mean that fracture widths and apertures have to be measured at multiple points along a fracture's length, even at a well-bore-diameter scale to generate meaningful average values (Liu et al., 2021). It is often informative to characterize fractures into distinct categories based on their forms and fill status (e.g., Mazdarani et al., 2023). Fractures tend to occur in different densities (frequencies) throughout a formation, often

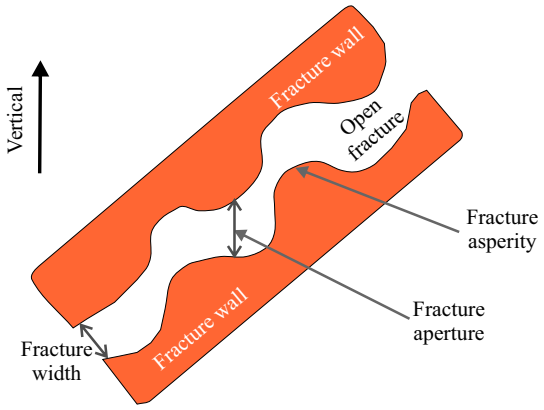

Fig. 3. Non-uniformity (surface roughness) and asperity typically characterizes rock formation fractures.

forming clusters in certain formation zones. Detecting such zones is often beneficial as they tend to coincide with high-permeability sections from which petroleum fluid recovery is greatest (Ajami et al., 2024).

The dips and strikes of fractures, and their azimuths (the angle measured clockwise from true north in the horizontal plane), as well as their apertures, other dimensions, and density of occurrence, can be derived from borehole images. For most forms of fracture analysis, it is best to calibrate BHI fracture interpretations with information derived from available rock cores, and thin sections taken from those cores to fully understand the form of microfractures. Statistical methods for evaluating fracture-spacing distributions are well established (Gillespie et al., 1999; Hooker et al., 2013) using coefficient of determination to assess the regularity of that spacing across a wellbore section of interest.

Fracture apertures are typically measured in the vertical direction (Nian et al., 2016, 2021), and their distributions are extrapolated through formations from wellbores measurements by a range of statistical techniques exploiting data from standard well logs (e.g., Ponziani et al., 2015), experimental measurements combined with simulations (e.g., Van Stappen et al., 2018) to provide some empirical guidance.

Fractures appear as distinct traces on FMI/FMS images depending upon their inclinations relative to the borehole trajectory (Fig. 4). Significantly, quasi-planar fractures do not appear as linear traces on borehole images but display sinusoidal forms. From those forms, particularly the wave amplitude, strike, dip, and azimuth can be relatively easily determined taking into account borehole trajectory. The appearance of mineral-filled fractures varies significantly on electrical and acoustic image logs, depending upon their acoustic and electrical properties and the contrast of those properties with the lithology of the fracture walls. Quantitative analysis of mineral-filled and partially-filled fractures can be conducted with BHI data combined with core and/or outcrop data to identify the types of fractures making the most beneficial contributions to production (Wang et al., 2023; Ajami et al., 2024).

Fig. 5 provides annotated examples of FMI images of inclined fractures transecting a wellbore. The left image in Fig. 5 displays a prominent planar, inclined fracture that crosses the sedimentary bedding planes. In the right image of Fig. 5, a discontinuous fracture is "bed-bound" (Luthi and SSouhaité, 1990). There tends to be a high-resistivity contrast between fractures invaded with drilling fluids compared to the rock-formation matrix, rendering quite narrow micro-fractures discernible on FMI/FMS images. However, the apparent apertures of such features on the BHI logs need to be calibrated with their widths as observed in corresponding cores. The same is true for fracture intensity measurements, which are typically expressed as the area of the fractures present per unit volume of formation (m^2/m^3). These should not be confused with fracture density measurements typically expressed as the number of fractures per unit of length of borehole or core using units of 1/cm or 1/m. Both fracture intensity and density tend to show positive correlations with formation permeability and can be predicted with relatively high accuracy by machine-learning methods using standard petrophysical well-log variables as inputs (Tabasi et al., 2022; Azadivash et al., 2024). Seismic-attributes from seismic datasets can also be combined with BHI data to extrapolate fault/fracture density/intensity analysis away from wellbores across prospective reservoirs (Babasafari et al., 2022).

5. Automated detection of fractures from borehole images

Computer-vision technologies together with CNN provide a means to potentially detect fractures directly from multiple segments of borehole images (Krizhevsky et al., 2017). Katterbauer et al. (2022) developed a deep-learning neural network to function in two stages. The first stage applied binary classification to determine the presence or absence of fractures in borehole image segments (8 cm long). The second stage applied a regression model to determine fracture density. In their current form such methods extensive image cropping, pre-processing, and/or annotation. Fast-region CNN has been used to detect breakouts and/or fractures from acoustic BHI tools (Dias et al., 2020). However, that method cannot be used to quantify the dimensions, inclinations, or apertures, of the fractures it detects. In contrast, mask region-based CNN (Mask R-CNN) models, with user-defined annotations have managed to generate more reliable automated BHI-feature detection (Liu et al., 2022).

Du et al. (2023) modified the Mask R-CNN pre-processing steps and demonstrated their method based on BHI images from six wells (Xinjiang field, China), examples of which are shown in Fig. 6. That model trained with a suite of user-annotated fracture examples was able to detect complete and partial fracture traces directly from annotated borehole images with training, validation, and testing datasets. This technique involved binary classification distinguishing user-annotated masked fracture zones from background regions of the images with no fractures. The model was further tested with deteriorated annotated masked images by applying Gaussian noise and/or blur and was able to detect fractures within the masks of those images with reasonable accuracy. Crucially, the redisplayed detected images. derived from un-

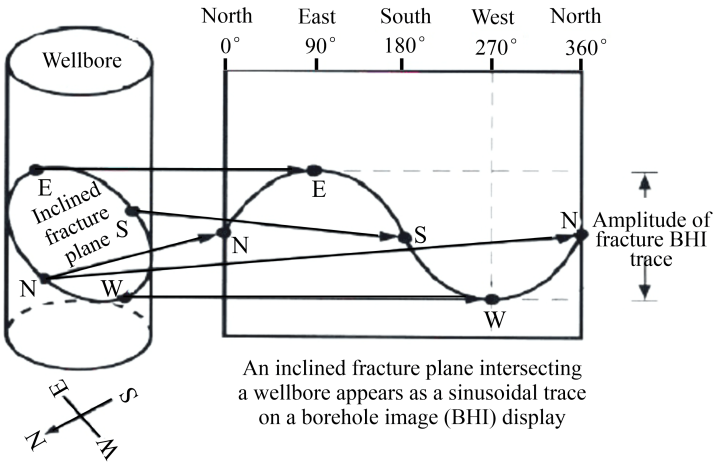

Fig. 4. Schematic diagram of a borehole image trace of a continuous planar feature oriented and inclined in specific directions transecting a wellbore's walls. Modified from Davarpanah et al. (2016).

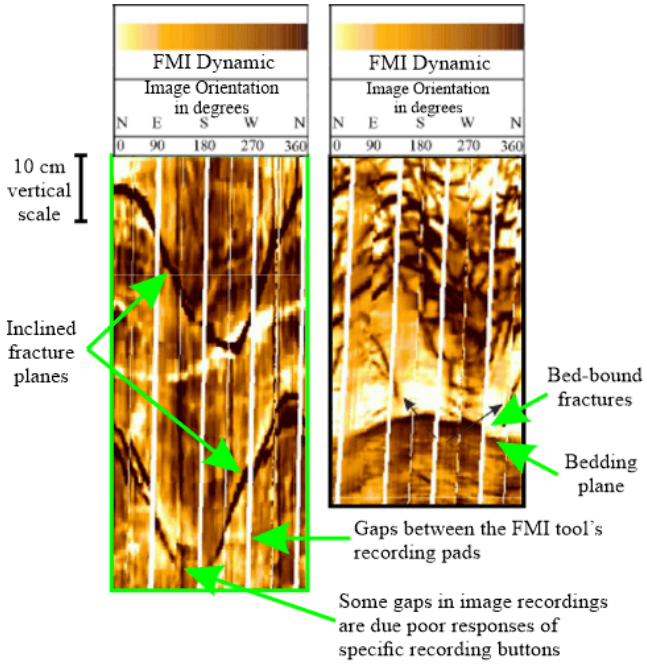

Fig. 5. FMI images displaying fracture traces. In the left image a continuous fracture crosses a bedding plane, whereas in the right image a discontinuous fracture occurs within a specific formation and does not transect the bedding planes. Modified from Nian et al. (2021).

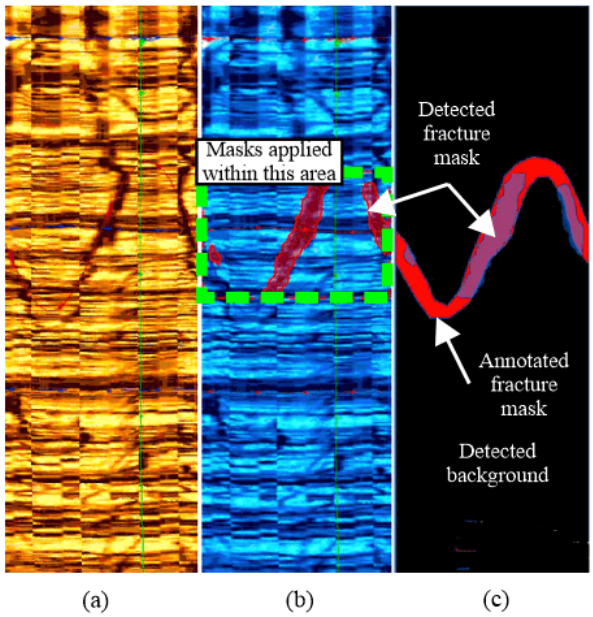

Fig. 6. Mask R-CNN borehole image processing to automate the detection and redisplay of fracture traces: (a) Initial borehole image, (b) detected and mask annotation applied to fracture traces and (c) annotated versus model detected masks of a fragmented sinusoidal borehole image fracture trace. Modified from Du et al. (2023).

masked test images, could be used to determine fracture apertures and orientations. The model is in development and requires further improvements to be able to detect features in BHI images recorded at different resolutions. If perfected, this technique offers the potential to substantially speed up the analysis of fracture traces (and other detected features) from long BHI image sections. Developments continue in deep-learning applications for automated fracture detection (Baraian et al., 2023; Olya et al., 2024).

6. Breakout analysis and stress orientation determination from acoustic borehole images

Stress-induced wellbore failures occur frequently during drilling operations. The determinations of principal stress directions are crucial for wellbore planning, and reservoir development planning (e.g., wellbore trajectories and fracture stimulation orientations. It is also necessary to establish long-term stability information for the wellbores servicing underground gas storage facilities (Heidbach et al., 2018; Wood, 2024). Wellbore stress failures occur as "breakouts"

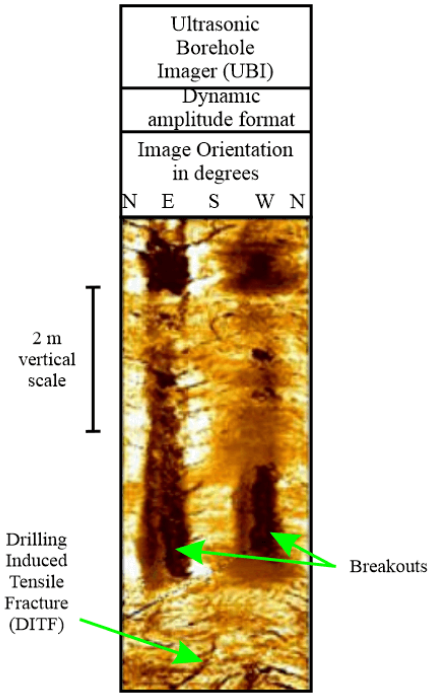

Fig. 7. Example UBI image of wellbore breakouts plus minor indications of DITF. Modified from Goswami et al. (2020).

and drilling-induced tensile fractures (DITF), which are readily distinguished on acoustic-tool borehole images (Fig. 7).

Acoustic BHI tools are widely used for breakout analysis due to their ability to provide complete three-hundred and sixty degree coverage of the wellbore walls and their lower operating costs to acquire BHI data across large depth intervals. High-resolution electric BHI tool images could also be used for this analysis but for many applications it is not cost effective to do so. Breakouts are typically aligned along the minimum horizontal stress ($S_{h\min}$) direction, as shown in Fig. 8, in near-vertical wellbores in tensional tectonic stress settings (Barton et al., 1988). They occur as gaps left by caved wellbore wall materials in circumstances where borehole stress magnitudes are greater than the compressive strength of the drilled formations. On the other hand, a DITF trajectory is more closely aligned with the maximum horizontal stress ($S_{H\max}$) direction. Breakouts typically appear in borehole images as two symmetrical failure features, aligned over specific depth intervals approximately 180° apart (Zoback et al., 2003) (Fig. 7).

The wellbore breakout relationships displayed in Fig. 8 are commonly exploited to calculate the magnitudes of the horizontal principal stresses (Zoback, 2009). BHI data are particularly effective at determining the horizontal principal stress directions when integrated with core data (Nie et al., 2013). $S_{h\min}$ magnitude can be separately determined by executing wellbore leak-off and/or mini-frac tests. Such tests do not though provide information regarding $S_{H\max}$ magnitude, so breakout analysis from borehole images offers a useful means to do so (Zoback et al., 2003) and is widely used for that purpose (Heidbach et al., 2018). At the edges of a breakout, compressional stress exerted by the wellbore exists in equilibrium with the rock formation's strength. It is that stress condition can be used to estimate $S_{H\max}$ magnitude. Several well-established empirical methods are available to do that (e.g., Barton et al., 1988; Zhou, 1994).

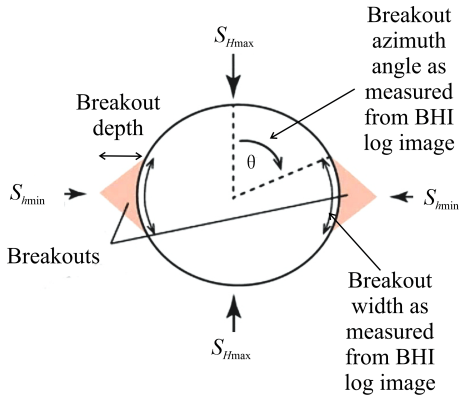

Fig. 8. Wellbore breakout orientations in relation to the prevailing principal stress directions ($S_{H\max}$ and $S_{h\min}$). θ is the azimuth angle between the SHmax direction and the nearest edge of the observed breakout. Modified after Huffman et al. (2016).

However, there are some uncertainties in using the empirical methods to predict $S_{H\max}$ magnitude from breakout measurements. For example, not all breakouts occur in the horizontal plane, which is an assumption made by these methods, breakouts tend to become deeper and wider as borehole diameter increases (Lin et al., 2020). In some wells the type of breakout and crucially their width vary substantially over relatively short vertical distances (Fig. 9), e.g., Harvey-1 well (Perth Basin, Australia) (Faraji et al., 2020). Hence, it is appropriate to validate SHmax magnitude determinations from BHI breakout measurements with additional poro-elastic information for the formations penetrated, such as static elastic modulus, static Poisson's ratio, and strain from rock core measurements (Nian et al., 2016). Machine learning methods can also assist in relating breakout dimensions to laboratory-derived rock strength measurements. For instance, Lin et al. (2020) developed a neural network model to predict $S_{h\min}$ from three easily measured inputs: Borehole-wall strength, vertical stress, and breakout width. It is also feasible to predict BHI breakout measurements with machine-learning methods using petrophysical well-log inputs to predict principal stress magnitudes (Ibrahim et al., 2021). Such models can then be applied to make predictions of stress magnitudes across a reservoir in wells where no BHI or core data is available.

Rose-diagram representations are usually used to display multiple breakout and fracture orientation determinations from borehole image measurements to indicate the uncertainty involved (Fig. 9).

7. Characterizing reservoir anisotropy using borehole image data

Rose-diagram representations are usually used to display multiple breakout and fracture orientation determinations from

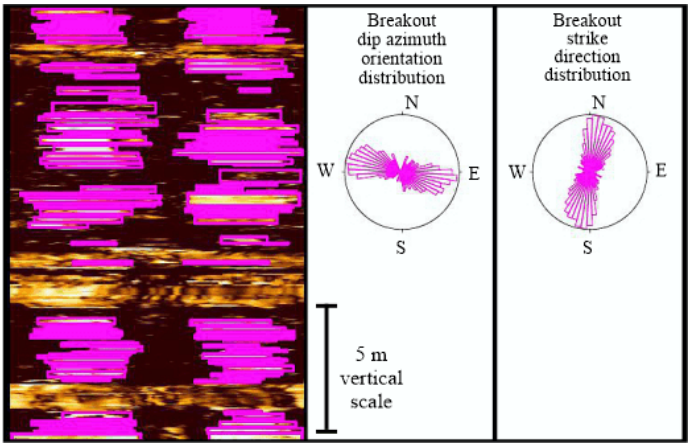

Fig. 9. Annotated CBIL image for a section of the Harvey-1 well highlighting the variability of breakout width measurements with depth. The purple box outlines (placed manually) delineate each identified breakout. Modified from Faraji et al. (2020).

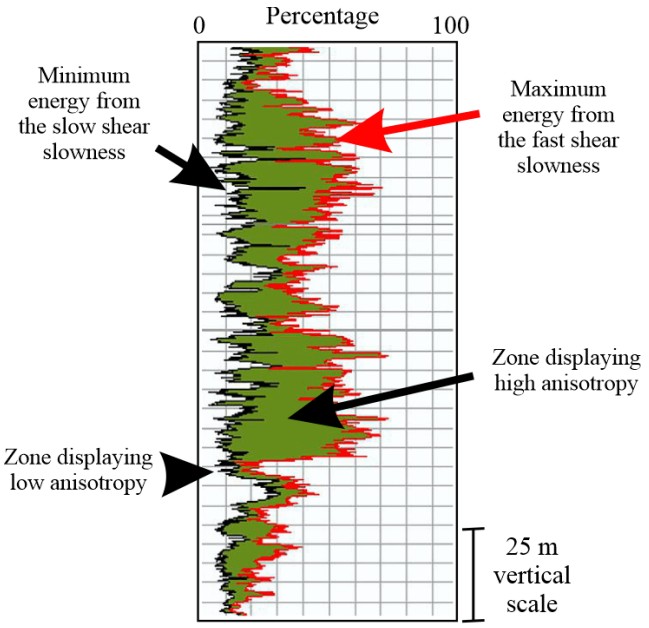

Fig. 10. Maximum energy and minimum energy traces versus depth, associated with the DSI fast and slow shear-wave slowness for a section of the South Pars Field Dalan/Kangan reservoir. Modified from Sadeqi et al. (2022).

borehole image measurements to indicate the uncertainty involved (Fig. 9). Acoustic shear wave data recorded by the DSI can be used to quantify reservoir anisotropy distributions, which can be very useful, especially for complex heterogeneous reservoir formations. The term "Anisotropy" used in the context of reservoir formation characteristics refers to directional variations in rock properties (Nelson, 2001), which is different from "heterogeneity" which is used to refer more generally to spatial variations in rock properties. Many carbonate reservoirs deposited in fluctuating platform depositional environments tend to be comprised of multiple microfacies, some of which have good reservoir properties, whereas other facies are tight and unproductive. Such formations are characterized by heterogeneity and anisotropy, with at least some of the higher reservoir-quality micro-facies exhibiting high degrees of anisotropy.

It is the comparison of the fast and slow DSI-recorded shear-wave components that makes it possible to quantify the extent of anisotropy at specific depths. Typically, there is a substantial difference between the recorded fast and slow shear-wave slowness in highly anisotropic zones. This can be usefully displayed in terms of the maximum versus minimum relative energies of the fast and slow shear-wave recordings, respectively. Sadeqi et al. (2022) evaluated DSI data from a wellbore penetrating the prolific gas-condensate Permo-Triassic carbonate Dalan/ Kangan reservoirs of South Pars gas-condensate field (Iran) to assess their relative anisotropy (Fig. 10). To do this reliably it is necessary to select the bandwidth of recorded shear wave data carefully and pre-process it to extract consistent information. For the Dalan/Kangan reservoir study sensitivity analysis revealed that the shear-wave bandwidth 2 to 4 kHz yielded the most reliable and consistent anisotropy results.

Shear-wave slowness differences can also be evaluated to determine the azimuth of anisotropy. The azimuth derived for the fast shear wave is usually interpreted as the azimuth of anisotropy for the filtered waveforms (Fig. 11), with multiple readings displayed in rose diagrams to provide an indication of uncertainty/confidence in those anisotropy azimuth readings at specific depths. The anisotropy orientations (~N60°E) derived for the Dalan/Kangan reservoir study are consistent with the alignment of fractures, and indicative of the $S_{H\max}$ direction. That direction is also consistent with regionally established structural orientations and $S_{H\max}$ directions (Zampetti et al., 2010).

8. Discussion: Integrated reservoir studies incorporating borehole image data

Ongoing studies of the Permo-Triassic Dalan/Kangan carbonate reservoir (offshore Iran) are progressively integrating sequence stratigraphy, lithology, poro-permeability data, and interpretations with combined FMI and DSI datasets (Fig. 12). Provisional results indicate that zones displaying high DSI-

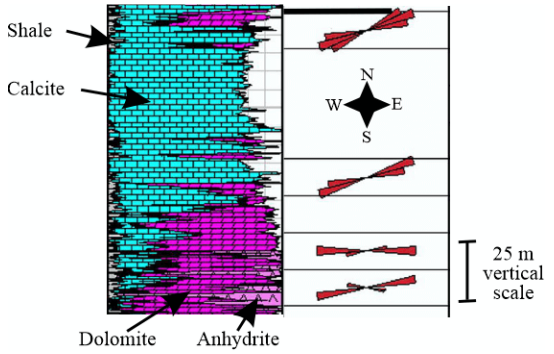

Fig. 11. Anisotropic zones and their orientations calculated from azimuths of the DSI fast shear wave for a portion of the South Pars Field Kangan K4 reservoir. Modified from Sadeqi et al. (2022).

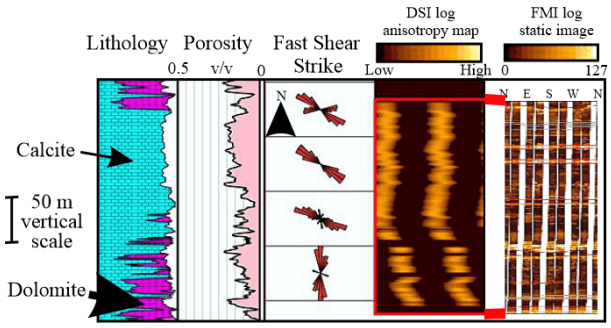

Fig. 12. Integrated display of lithology, porosity, fast shear wave strike direction (DSI), anisotropy map (DSI; bright color indicates high anisotropy), porous versus tight zones (static FMI image) for a portion of the Upper Dalan formation.

recorded anisotropy and high FMI-recorded heterogeneity are closely related to highstand (regressive) sedimentary tracts and associated with high reservoir quality (porosity/ permeability). Such zones can be readily distinguished from transgressive, lowstand (transgressive) tracts associated with low reservoir quality. In detail, the most (visible) conductive zones on the FMI images tend to be the most porous/permeable, whereas most resistive zones tend to more highly cemented exhibiting low porosity/ permeability. Hence, the DSI and FMI data provide complementary insights into reservoir characteristics.

There is potential to convert the fast and slow DSI shear-wave depth variations (e.g., Fig. 10) into a relative anisotropy index. Such an index then has the potential of being predicted by machine learning using a basic suite of petrophysical well logs or mud-log drilling variables. In that way, DSI data from just a few wells could be used to extend anisotropy analysis across an entire reservoir using data from wells that have not been cored or surveyed with DSI logs. Further studies on a range of heterogeneous/anisotropic reservoirs are required to assess the reservoir-characterization value of such an approach.

The results of the integrated analysis illustrated in Fig. 12 provide indications of the potential benefit of adopting a more integrated reservoir characterization approach involving both acoustic and electrical BHI datasets. This approach is not just useful for heterogeneous carbonate reservoirs, heterogeneous and highly fractured shale and coal reservoirs could also be more comprehensively characterized in this way.

BHI logs are sometimes run in vertical coal-bed methane (CBM) wells but access for these logging tools in highly deviated, short-radius, narrow-diameter multi-lateral CBM wells is difficult and has restricted their deployment. However, the information BHI logs can potentially provide for relatively tight (permeability < 10 mD) sporadically fractured CBM wells is highly relevant to their characterization. For example, identifying the distributions and orientations of fractures and cleats to guide wellbore positioning and lateral-wellbore trajectories. Zhou et al. (2022) presented electrical-BHI data for a 1,900 m horizontal lateral section of a Bowen Basin (Australia) coal seam, representing the first time that such a tool had been run in such a complex well in that basin. They used the data obtained to refine the discrete fracture network model for that area of the coal basin, refining the fracture/fault distribution and orientation interpretations from available 3D seismic and adjacent vertical wells. The BHI data analysis revealed that fracture/cleat orientations progressively changed direction from NE to NW across the studied area, something that was not observable from the existing data. Moreover, fracture/cleat orientation changes correlated with a decrease in permeability and a reduction in natural gas productivity, a trend that the BHI data was able to quantify and relate to directional permeability.

The results obtained for the Dalan/Kangan carbonate and the Bowen Basin CBM heterogeneous reservoirs highlight the benefits of integrating BHI data with other available reservoir data to provide more comprehensive reservoir characterizations.

9. Conclusions

BHI well-log tools represent a well-established technology that has been exploited successfully for more than three decades to provide a range of quantitative measurements relating to specific reservoir characteristics. The electrical BHI tools, such as the FMI, are routinely used for high-resolution fracture distribution and characterization analysis, calibrated with core measurements. On the other hand, acoustic borehole images are routinely used for breakout studies to determine the directions and magnitudes of the local principal horizontal stresses. However, BHI datasets contain a wealth of additional information that is generally not exploited to its full potential in terms of the contributions it could make to comprehensive reservoir characterization studies.

A case is made for the additional reservoir-characterization benefits provided by incorporating BHI datasets with sequence stratigraphy, lithology, poro-permeability, and seismic datasets. An approach that has been successfully demonstrated by a few recent studies. Such an approach is particularly relevant for highly heterogeneous/ anisotropic reservoirs, such as many carbonate, shale, and coal formations. Combining the information from both electrical and acoustic borehole images, particularly the DSI, provides complementary insights into such complex reservoirs. Recent machine learning developments have substantially expanded the interpretation

possibilities for BHI datasets, including automated fracture detection. Moreover, the ability to predict BHI measurements from standard petrophysical well-log and drilling mud-log datasets extends their findings across reservoirs using the more limited data available in the majority of existing wellbores.

Acknowledgements

Paper to accompany presentation delivered at the First Geo-Energy Frontier Forum, April 19-22, 2024, Wuhan, China.

Supplementary file

https://doi.org/10.46690/ager.2024.06.04

Conflict of interest

The author declares no competing interest.

References

Ajami, M., Davoodi, S., Asgari, K., et al. The impact of fractures and planar structures on the quality of the Upper Jurassic Mozduran reservoir, Kopet Dagh Basin (Northeast Iran). Journal of Asian Earth Sciences, 2024, 267: 106167.

Azadivash, A., Soleymania, H., Seifirad, A., et al. Robust fracture intensity estimation from petrophysical logs and mud loss data: A multi-level ensemble modeling approach. Journal of Petroleum Exploration and Production Technology, 2024, in press, https://doi.org/10.1007/s13202-024-01820-9.

Babasafari, A. A., Chinelatto, G. F., Vidal, A. C. Fault and fracture study by incorporating borehole image logs and supervised neural network applied to the 3D seismic attributes: A case study of pre-salt carbonate reservoir, Santos Basin, Brazil. Petroleum Science and Technology, 2022, 40(12): 1492-1511.

Baraian, A., Kellokumpu, V., Tomi, R., et al. Automatic fracture detection and characterization in borehole images using deep learning-based semantic segmentation. Paper Presented at the 18th International Joint Conference on Computer Vision, Imaging and Computer Graphics Theory and Applications (VISIGRAPP), Lisbon, Portugal, 19-21 February, 2023.

Barton, C. A., Zoback, M. D., Burns, K. L. In-situ stress orientation and magnitude at the Fenton Geothermal Site, New Mexico, determined from wellbore breakouts. Geophysical Research Letters, 1988, 15(5): 467-470.

Boro, H., Rosero, E., Bertotti, G. Fracture-network analysis of the Latemar Platform (northern Italy): Integrating outcrop studies to constrain the hydraulic properties of fractures in reservoir models. Petroleum Geoscience, 2014, 20: 79-92.

Bourke, L. T., Delfiner, P., Trouiller, J. C., et al. Using formation microscanner images. The Technical Review (Schlumberger), 1989, 37(1): 16-40.

Brown, J., Davis, B., Gawanker, K, et al. Imaging: Getting the picture downhole. Schlumberger Oilfield Review (September), 2015, 27(2): 4-21.

Chongqing Gold Mechanical & Electrical Equipment Co., Ltd. Geophysical wireline borehole imaging equipment. Chongqing Gold Mechanical & Electrical Equipment Co., Ltd., 2024.

Columbia University. Dipole Sonic Imager Tool (DSI-2; SLB). Columbia University, 2024.

Davarpanah, A., Kakoli, M., Ahmadi, H. Analysis of fractured reservoir structure by interpretafion of FMI and VSP logs. Journal of Marine Science: Research & Development, 2016, 6: 216.

Dias, L. O., Bom, C. R., Faria, E. L., et al. Automatic detection of fractures and breakouts patterns in acoustic borehole image logs using fast-region convolutional neural networks. Journal of Petroleum Science and Engineering, 2020, 191: 107099.

Du, L., Lu, X., Li, H. Automatic fracture detection from the images of electrical image logs using Mask R-CNN. Fuel, 2023, 351: 128992.

Ekstrom, M. P., Dahan, C. A., Chen, M. Y., et al. Formation imaging with microelectrical scanning arrays. Paper SPWLA 1986 Presented at the SPWLA 27th Annual Logging Symposium, Houston, Texas, 9-13 June, 1986.

Esmersoy, C., Kane, M., Boyd, A., et al. Fracture and stress evaluation using dipole-shear anisotropy logs. Paper SPWLA 1995 Presented at the SPWLA 36th Annual Logging Symposium, Paris, France, 26-29 June, 1995.

Fanchi, J. R. Fracture and shale systems, in Principles of Applied Reservoir Simulation, edited by John R. Fanchi, Elsevier, USA, pp. 241-256, 2018.

Faraji, M., Rezagholilou, A., Ghanavati, M., et al. Breakouts derived from image logs as an aid in estimation of the magnitude of maximum horizontal stress: A case study from Perth Basin, Western Australia. Advances in Geo-Energy Research, 2020, 5(1): 8-24.

Gillespie, P. A., Johnston, J. D., Loriga, M. A., et al. Influence of layering on vein systematics in line samples, in Fractures, Fluid Flow and Mineralization, edited by McCaffrey, K. J. W., Lonergan, L., Wilkinson, J. J. Geological Society, London, pp. 35-56, 1999.

Goswami, D., Hazarika, P., Roy, S. In situ stress orientation from 3 km borehole image logs in the Koyna Seismogenic Zone, Western India: Implications for transitional faulting environment. Tectonics, 2020, 39: e2019TC005647.

Haldorsen, J. B. U., Johson, D. L., Plona, T., et al. Borehole acoustic waves. Schlumberger Oilfield Review, 2006, 18(1): 34-43.

Halliburton. X-tended Range Micro Imaging (XRMI™) tool, 2024.

Hawez, H. K., Sanaee, R., Faisal, N. H. A critical review on coupled geomechanics and fluid flow in naturally fractured reservoirs. Journal of Natural Gas Science and Engineering, 2021, 95: 104150.

Heidbach, O., Rajabi, M., Cui, X., et al. The World Stress Map database release 2016: Crustal stress pattern across

scales. Tectonophysics, 2018, 744: 484-498.

Hooker, J. N., Laubach, S. E., Marrett, R. Fracture-aperture size- frequency, spatial distribution, and growth processes in strata-bounded and non-strata-bounded fractures, Cambrian Meson Group, NW Argentina. Journal of Structural Geology, 2013, 54: 54-71.

Hosseinzadeh, S., Kadkhodaie, A., Wood, D. A., et al. Discrete fracture modeling by integrating image logs, seismic attributes, and production data: A case study from Ilam and Sarvak Formations, Danan Oilfield, southwest of Iran. Petroleum Exploration and Production Technology, 2023, 13(4): 1053-1083.

Huffman, K. A., Saffer, D. M., Dugan, B. In situ stress magnitude and rock strength in the Nankai accretionary complex: a novel approach using paired constraints from downhole data in two wells. Earth, Planets and Space, 2016: 68(1): 123.

Ibrahim, A. F., Gowida, A., Ali, A., et al. Machine learning application to predict in-situ stresses from logging data. Scientific Reports, 2021, 11(1): 23445.

IODP. Ultrasonic Borehole Imager (UBI; SLB trademark). International ocean drilling program, 2024.

Ismail, A., Farshid, T., Azadbakht, S., et al. Identification of natural fractures in shale gas reservoirs using fracture signature function and machine learning models. Unconventional Resources, 2024, 4: 100069.

Katterbauer, K., Al Qasim, A., Al Shehri, A., et al. Smart detection of fractures in formation image logs for enhanced CO_2 storage. Science and Technology for Energy Transition, 2022, 77(21): 1-7.

Khoshbakht, F., Azizzadeh, M., Memarian, H., et al. Comparison of electrical image log with core in a fractured carbonate reservoir. Journal of Petroleum Science and Engineering, 2012, 86: 289-296.

Krizhevsky, A., Sutskever, I., Hinton G. E. ImageNet classification with deep convolutional neural networks. Communications of the ACM, 2017, 60(6): 84-90..

LandSea. Circumferential Borehole Imaging Logging Tool (CBITTM), 2024.

Lin, H., Oh, J., Canbulat, I., et al. Experimental and analytical investigations of the effect of hole size on borehole breakout geometries for estimation of in situ stresses. Rock Mechanics and Rock Engineering, 2020, 53(2): 781-798.

Liu, J., Yang, H., Bai, J., et al. Numerical simulation to determine the fracture aperture in a typical basin of China. Fuel, 2021, 283: 118952.

Liu, Y., Liao, G., Xiao, L., et al. Automatic fracture segmentation and detection from image logging using Mask R-CNN. Paper SPWLA 2022 0115 Presented at the SPWLA 63rd Annual Logging Symposium, Stavanger, Norway, 11-15 June, 2022.

Luthi, S. M., Souhaité, P. Fracture apertures from electrical borehole scans. Geophysics, 1990, 55(7): 821-833.

Mazdarani, A., Kadkhodaie, A., Wood, D. A., et al. Natural fractures characterization by integration of FMI logs, well logs and core data: A case study from the Sarvak Formation (Iran). Journal of Petroleum Exploration and Production Technology, 2023, 13(5): 1247-1263.

Nabiei, M., Yazdjerdi, K., Soleimany, B., et al. Analysis of fractures in the Dalan and Kangan carbonate reservoirs using FMI logs: Sefid-Zakhur gas field in the Fars Province, Iran. Carbonates and Evaporites, 2021, 36(2): 28.

Nelson, R. A. Evaluating fractured reservoirs, in Geologic Analysis of Naturally Fractured Reservoirs, edited by R. A. Nelson, Elsevier, Houston, pp. 1-100, 2001.

Nian, T., Wang, G., Tan, C., et al. Hydraulic apertures of barren fractures in tight-gas sandstones at depth: Image-core calibration in the Lower Cretaceous Bashijiqike Formation, Tarim Basin. Journal of Petroleum Science and Engineering, 2021, 196: 108016.

Nian, T., Wang, G., Xiao, C., et al. The in situ stress determination from borehole image logs in the Kuqa Depression. Journal of Natural Gas Science and Engineering, 2016, 34: 1077-1084.

Nie, X., Zou, C., Pan, L., et al. Fracture analysis and determination of in-situ stress direction from resistivity and acoustic image logs and core data in the Wenchuan Earthquake Fault Scientific Drilling Borehole-2 (50-1,370 m). Tectonophysics, 2013, 593: 161-171.

Ng, C. S. W., Amar, M. N., Ghahfarokhi, A. J., et al. A survey on the application of machine learning and metaheuristic algorithms for intelligent proxy modeling in reservoir simulation. Computers & Chemical Engineering, 2023, 170: 108107.

Olya, B. A. M., Mohebian, R., Bagheri, H., et al. Toward real-time fracture detection on image logs using deep convolutional neural network YOLOv5. Interpretation, 2024, 12(2): SB9-SB18.

Pachineelam, S., Paluri, B. S., Mudigonda, A. S. K., et al. Evaluation of stress anisotropy of the formation by utilizing dipole shear sonic imager (DSI*), formation micro imager (FMI*) and density log-a case study on Kanawara Field, South Cambay Basin, India. Paper Presented at the International Petroleum Technology Conference, Bangkok, Thailand, 15-17 November, 2011.

Ponziani, M., Slob, E., Luthi, S., et al. Experimental validation of fracture aperture determination from borehole electric microresistivity measurements. Geophysics, 2015, 80(3): D175-D181.

Qobi, L., De Kuijper, A., Tang, X. M., et al. Permeability determination from Stoneley waves in the Ara Group carbonates, Oman. GeoArabia. 2001, 6(4): 649-666.

Sadeqi, M., Manaman, N. S., Kadkhodaie, A., et al. The effect of frequency bandwidth on DSI anisotropy evaluation. Journal of Applied Geophysics, 2022, 201: 104641.

SLB. Fullbore formation micro-imager (FMI), 2024

Tabasi, S., Tehrani, P. S., Rajabi, M., et al. Optimized machine learning models for natural fractures prediction using conventional well logs. Fuel, 2022, 326: 124952.

Tóth, E., Hrabovszki, E., Tóth, T. M. Using geophysical log data to predict the fracture density in a claystone host rock for storing high-level nuclear waste. Acta Geodaetica et Geophysica, 2023, 58: 35-51.

Vahle, C., Veselovsky, Z., Ruehlicke, B. Detailed geological

reservoir characterisation using an integrated analysis of borehole image logs. Paper Presented at the 1st Geoscience & Engineering in Energy Transition Conference, Strasbourg, France, 16-18 November, 2020.

Van Stappen, J. F., Meftah, R., Boone, M. A., et al. In situ triaxial testing to determine fracture permeability and aperture distribution for CO_2 Sequestration in Svalbard, Norway. Environmental Science & Technology, 2018, 52(8): 4546-4554.

Vijouyeh, A. G., Kadkhodaie, A., Sedghi, M. H., et al. Identification of high potential zones for hydrocarbon production based on fracture aperture estimation using hybridised intelligent systems: Datasets and Supplementary Materials, Mendeley Data, 2023.

Wang, Q., Narr, W., Laubach, S. E. Quantitative characterization of fracture spatial arrangement and intensity in a reservoir anticline using horizontal wellbore image logs and an outcrop analogue. Marine and Petroleum Geology, 2023, 152: 106238.

Weatherford. Compact™ Microresistivity Tool, 2024

Wood, D. A. Well integrity for underground gas storage relating to natural gas, carbon dioxide, and hydrogen, in Sustainable Natural Gas Drilling: Technologies and Case Studies for the Energy Transition, edited by D. A. Wood and J. Cai, Elsevier, Amsterdam, pp. 551-576, 2024.

Wood, D. A., Cai, J. Coal-bed methane reservoir characterization using well-log data, in Sustainable Geoscience for Natural Gas Subsurface Systems, edited by D. A. Wood and J. Cai, Elsevier, Huston, pp. 243-274, 2022.

Zampetti, V., Borkhataria, R., Vroon, M. Multi-scale assessment of the Middle Eastern Permo-Triassic Khuff Carbonate: Structural evolution and its impact from reservoir properties. Paper Presented at AAPG GEO Conference, Manama, Bahrain, 7-10 March, 2010.

Zhang, J., Nie, X., Xiao, S., et al. Generating porosity spectrum of carbonate reservoirs using ultrasonic imaging log. Acta Geophysica, 2018, 66: 191-201.

Zhou, F., Oraby, M., Luft, J., et al. Coal seam gas reservoir characterisation based on high-resolution image logs from vertical and horizontal wells: A case study. International Journal of Coal Geology, 2022, 262: 104110.

Zhou, S. A program to model the initial shape and extent of borehole breakout. Computers & Geosciences, 1994, 20(7-8): 1143-1160.

Zoback, M. D. Reservoir Geomechanics. Cambridge, United Kingdom, Cambridge University Press, 2009.

Zoback, M. D., Barton, C. A., Brudy, M., et al. Determination of stress orientation and magnitude in deep wells. International Journal of Rock Mechanics Mining Sciences, 2003, 40(7-8): 1049-1076.